2019

Structure Difference and Implication to Assembly Morphology Control of Rous Sarcoma Virus Capsid Protein

John Hastings
University of Central Florida

STRUCTURE DIFFERENCE AND IMPLICATION TO ASSEMBLY MORPHOLOGY CONTROL OF ROUS SARCOMA VIRUS CAPSID PROTEIN

By

JOHN HASTINGS

A thesis submitted in partial fulfillment of the requirements
for the Honors in the Major Program in Physics
in the College of Sciences
in the Burnett Honors College
at the University of Central Florida
Orlando, Florida

Fall Term, 2018

Thesis Chair: Dr. Bo Chen

ABSTRACT

Rous Sarcoma Virus (RSV) is an avian retrovirus with an enclosing capsid protein (CA) shell. RSV CA is studied due to its similar molecular structure to other retrovirus capsid proteins such as Human Immunodeficiency Virus (HIV). In this project, turbidity assay is used to track the assembly process of RSV CA, while solid state nuclear magnetic resonance (ssNMR) is used to probe the CA structure at a site specific level and investigate the morphology of the spherical structure of the I190V mutated strain of RSV CA. The I190V mutant is a naturally occurring mutation and is able to form into roughly uniform spheres, where the wild type RSV CA cannot form as pure spheres as possible. Turbidity assay results of the mutated RSV CA revealed a lack of a noticeable lag time before assembly began, as well as, a prolonged time period to reach saturation when compared to the wild-type RSV CA. Using ssNMR, and the TALOS-N program the torsion angles of the protein backbone were found. Using Ramachandran plots, it was found that the mutation of the 190th residue from Isoleucine to Valine caused a changed in the secondary structure of residues, from α-helix to β-sheet and vice versa. These changes were concentrated at the loops between select interfaces of helices that make up the structure of RSV CA. In particular, between helices 4 (residues 65-85), 8 (residues 165-177), and 11 (residues 215-225). The differing secondary structure in the mutant RSV CA was supported by the overlaying of the NMR spectra of the wild-type RSV CA on to the spherically assembled mutant RSV CA. It can be concluded that the spherical assembly of the mutated RSV CA displays noticeable differences in assembly and overall structure when compared to the wild-

type RSV CA.

ACKNOWLEDGMENTS

The base acquisition of much of the data used in this thesis was found by a previous student under Dr. Bo Chen, Xin Qiao. Xin prepared the buffers used in the assembly process for the mutated RSV CA, as well as, acquired and processed the NMR spectra of the mutated RSV CA.

TABLE OF CONTENTS

LIST OF FIGURES

LIST OF TABLES

LIST OF IMAGES

INTRODUCTION

The main aim of this research is to study the structure and assembly of Rous Sarcoma Virus (RSV) capsid protein (CA). In this project, turbidity assay is used to track the assembly process, while ssNMR is used to probe the CA structure at a site specific level and investigate the morphology of the spherical structure of the I190V mutated strain of RSV CA. The I190V mutant is able to form into roughly uniform spheres, where the wild type RSV CA cannot form as pure spheres as possible. Studying the I190V mutant will help us selectively have a pentamer formation rather than the tubular formation of RSV CA which comprises of pure hexamers. This gives us different information about the assembly morphology.

RSV is an avian retrovirus originally discovered by Peyton Rous in 1911 [1]. Retroviruses are ubiquitous infectious agents that have been found in many species, ranging from simple eukaryotes to humans. Their replication is characterized by converting the RNA genetic information into the DNA of their host cell. Retroviruses have been of great interest due to their association with important diseases, including cancers, HIV, and neurologic diseases [4]. Retroviruses are grouped in several different genera such as B-type, C-type, D-type, HTLV/BLV, and lentiviruses. RSV is a monomeric C-type retrovirus, meaning it contains a central, spherical core [7]. The assembly of retroviruses is directed by a single protein, Gag. Several thousand copies of the Gag polyproteins recognize and capture viral RNA, and then assemble and bud into enveloped immature virus particles, with their N terminal domain (NTD) being associated with the lipid bilayer and their C terminal domain (CTD) contacting the RNA genome in the virion interior [2,3]. Enveloped refers to having a lipid bilayer membrane

encasing the viral RNA. Not all viruses will have this lipid membrane. Simultaneous to budding, in a process termed maturation, the Gag protein is cleaved by the viral protease into the structural proteins found in the infectious virus. These include the matrix protein (MA), capsid protein (CA), nucleocapsid protein (NC), spacer peptide (SP) and the protease (PR). The CA reorganizes to form the shell of the mature viral core [2,3].

The CTD contains a stretch of 20 residues near its N terminus that has been termed the major homology region (MHR) due to its high level of conservation among nearly all genera of retroviruses [3]. The 190th residue of RSV CA which has been mutated is not in the MHR. The structure of each of the individual residues of the capsid proteins can be investigated using Nuclear Magnetic Resonance (NMR) probing. NMR operates on the principle that the resonance frequencies of nuclei are intimately correlated with the chemical bonding and protein conformation [11]. This project specifically applies Solid State Nuclear Magnetic Resonance (ssNMR) to determine the structure of RSV CA in its spherical assembly.

This thesis will be aimed at understanding the assembly kinetics of the RSV CA, as well as, the structure of the I190V mutation of RSV CA investigated by ssNMR probing. By gathering more information on the structure and kinetics of RSV CA assembly, new insights into the behavior of RSV CA will be made known. Our results will determine the kinetic constants and binding affinities of RSV CA in its assembly and the secondary structure of the I190V mutant in its spherical assembly. By comparing with prior tubular assembly structure, the difference of RSV CA in the spherical structure will be revealed, which will help understand the formation of different curvatures in

authentic RSV capsid.

Over a broader scope, this knowledge will add to our understanding of the assembly mechanism of various retrovirus capsids, especially those related to important diseases, such as human immunodeficiency virus (HIV), T-lymphotropic virus type 1 (HTLV-1), and T-lymphotropic virus type 2 (HTLV-II) [3].

Literature Review

Retroviruses are comprised of two main components: an inner core surrounded by an outer envelope, formed of a lipid bilayer membrane. The inner core is formed by an outer shell of capsid proteins (CA) that surround the dimeric RNA genome, along with other molecules such as NC proteins [5]. Capsid proteins of RSV exhibit a high degree of polymorphism. The capsids are best described as protein lattices, organized following similar principles as fullerene carbon structures, with subunits arranged in hexamers interspersed with pentamers. The wide range of capsid morphologies is due to a lack of regular spacing between these pentamers. The structure of the two folded domains (NTD and CTD) of CA is highly conserved and the capsid assembly pathway is thought to be conserved as well. This is amongst all retroviruses. In the case of RSV, in vitro assembly of the highly polymorphic capsid protein has been observed to be a well-behaved nucleation-driven process [6]. What exactly this nucleus is, is still unknown.

To gain a more complete picture of capsid proteins it must first be understood what exactly proteins are. All proteins are made up of amino acids linked together by peptide bonds into a polypeptide chain [8]. Alpha amino acids are made up of an amino group, a carboxyl group, a hydrogen atom, and a side chain, all bonded to a central α-carbon atom. This configuration is shown in Image 1. During formation of the polypeptide chain, each amino acid loses two hydrogen atoms and one oxygen atom (OH from the carboxyl group and H from the amino group). Therefore, the convention is to use the term “amino acid residue” when referring to the amino acids in a polypeptide chain.

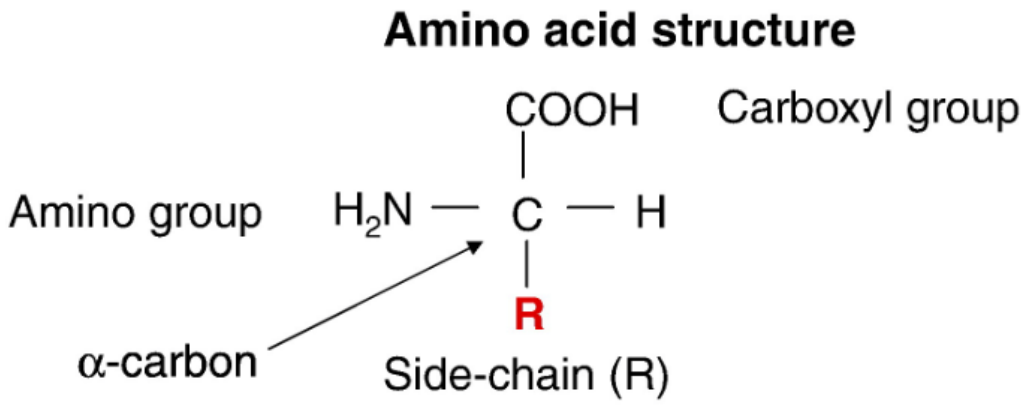

Image 1. The structure of an amino acid [9].

There are 20 universal amino acids that appear in almost all proteins. These are listed in Image 2. The I190V mutation of the RSV CA replaces one of these universal amino acids, Isoleucine, with a Valine.

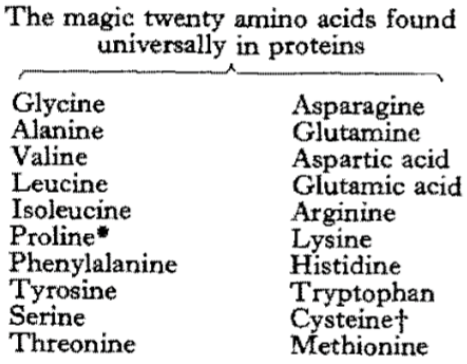

Image 2. The 20 amino acids commonly occurring in proteins [8].

What makes each amino acid unique is the side chain [8]. The capsid protein of RSV has 237 amino acids [10]. While we know how retrovirus CA's on a general scale are formed (see the introduction of this proposal), all the details into the assembly of RSV's CAs are not known. RSV CA has been shown to assemble into several configurations [6]. This project looks specifically into the assembly of RSV CA into spherical shells, more specifically why does the RSV CA I190V mutant assemble into spheres? We investigate this question through turbidimetric assay.

Turbidity assays can be used to track the assembly process of capsid proteins [6]. Several factors such as concentration of protein or the specific salt solutions used in the assay, affect assembly and subsequent turbidity [6]. Turbidity is essentially the scattering of light, so as the protein begins to assemble and form more and more structures, these structures are able to scatter more light, thus increasing turbidity. It is with these factors in mind that the parameters for this project have been chosen. Through line and curve fitting of several turbidimetric data plots we can find the dissociation constants associated with the four interfaces of CA polymerization. These four interfaces are: the dimerization of monomers, trimerization of dimers, formation of hexamers from trimers of dimers, and the polymerization of hexamers [3]. The monomers of RSV CA form into CA-CA dimers which will form trimers of CA-CA dimers. These trimers of dimers will group together to form a hexameric lattice with interspersed pentamers, that will form the spherical CA shell [3]. The exact reasons that the I190V mutant assembles into a spherical shell, and the exact process and kinetics in which it does so is what this project aims to uncover.

Through the use of ssNMR, more supporting information into the structure of the I190V mutant can be found. Through NMR we are able to detect chemical shift deviations, measured in parts per million (ppm). These deviations are very precise, sensitive, indicators of protein secondary structures and thus represent a powerful medium to detect residual secondary structures in proteins, in our case, in RSV's CA [10]. In concise manner, inside the nucleus of an atom, each proton and neutron has spin +1/2 or -1/2. In atoms with even numbers of protons and neutron, these spins are cancelled out so that the nucleus of the atom has no net spin. The nuclei of ^{1}H, ^{13}C, and

^{15}N have net spin of ½. A local magnetic field is produced from the interaction of two nearby nuclei. The interaction of one nuclear spin with the magnetic field produced by the other nuclear spin causes a dipolar interaction. The dipole-dipole interaction between two dilute spin, S = 1/2, nuclei is shown as a Pake doublet in NMR spectra, with the frequency difference not only a function of the distance between the two nuclei but also the angle of the external magnetic field to the inter-nuclear vector [12]. This project uses a technique called magic-angle spinning (MAS), which spins a sample at the magic angle of 54.74° with respect to the external magnetic field. In solution NMR, the rapid isotropic motions of molecules result in efficient averaging out of the orientational dependence of nuclear magnetic reactions. This leaves only the isotropic component detectable. In solid state, such is the case of this experiment, MAS is used to eliminate the orientational dependence of the NMR anisotropic interactions in solid-phase samples. This has been found to occur best at the angle of 54.74° [15]. ssNMR also utilizes a technique, known as cross polarization, in which polarization from abundant spins (I) such as ^{1}H are transferred to dilute spins (S) such as ^{13}C or ^{15}N. This requires that nuclei are dipolar coupled to one another. The anisotropy of nuclear spin interactions produces the NMR spectra. This anisotropic dipole-dipole interaction provides information into geometrical parameters that are translated into structural information of the molecule [12].

Whether or not solid-state NMR or solution NMR are used, structure determination of proteins is based on the same general principles. In this experiment, the assembly is not soluble in solution. The assembly precipitates from the protein solution, and therefore cannot be analyzed using solution NMR. This solid state NMR is used.

Through the use of isotopic labels and multidimensional NMR experiments, or the measuring of spectral parameters associated with individual resonances, such as dipolar couplings, or chemical shift frequencies, the assignment of all resonance to specific sites in the protein measured in ppm, the resolution of resonances is found and then the calculation of structures can be completed [12]. Chemical shift is used to spot differences between chemically inequivalent sites which is caused by changes to the local electronic environment surrounding the nucleus [13]. When electrons orbit around their nucleus, they produce a magnetic field, much like how a current in a wire will produce a magnetic field around the wire. When introduced to external magnetic field, B_0, the atom's magnetic field will run anti-parallel to the external magnetic field. This causes the electron-generated magnetic moment to be opposite in direction when compared to the externally produced magnetic moment. The conflict of direction between these two magnetic moments reduces the net magnetic moment affecting the proton in the atom. Thus, the magnetic field produced by the electron orbiting the nucleus can either enhance or diminish the external magnetic field, changing the energy needed to promote a nuclear transition. Protons with different chemical environments will yield resonance frequencies perturbed from the frequency defined by the external magnetic field. This electronic effect can be included in the Larmor frequency: $\omega_0=\gamma B_0$, where γ is the gyromagnetic ratio. It is common to define chemical shift in terms of the difference between the Larmor frequency of a nucleus being investigated and a reference nucleus [11, 13]. This is the basis of chemical shift.

With the information gathered through turbidimetric assay and ssNMR probing, this project aims to uncover the curvature formation mechanism that leads to spherical shaped RSV CA.

METHODOLOGY

The questions that will be investigated through this project include the following: What are the kinetics of spherical assembly of RSV CA? For example, how long does assembly take at given parameters? How long is the lag period for assembly to begin at the tested concentration with 500 mM sodium phosphate buffer at pH 8.0? What is the diameter of the assembled sphere? Other questions that this project seeks to investigate include: What are the chemical shifts for each of the 237 residues of the RSV CA I190V mutant? How do these shifts affect the structure of the capsid protein and how does this structure affect the capsid proteins behavior?

The procedures that will be used to investigate these questions have been broken down into four tasks.

The protein samples tested in this thesis were prepared by previous student Xin Qiao. The sample used to in the NMR spectra was acquired and processed by Xin Qiao. Residue peaks of the spherically assembled mutated RSV CA were found with help from current student Tyrone Thames.

Task 1: Obtain Desired Concentration of RSV CA

An initial amount of RSV CA I190V mutant was be obtained from a supply made in the previous work of Dr. Xin Qiao. Using the “A280 Absorbance” program of a spectrophotometer, the NanoDrop2000, concentrations of the supply of protein will be assessed. Once, the concentration of RSV CA is known, a total amount of 6mg of protein will be pipetted into a 20mL capacity Vivaspin20 centrifuge tube with a 3,000 molecular weight cutoff (MWCO) polyethersulfone (PES) membrane. The protein will be centrifuged using a Sorvall Super T21 Centrifuge at 4 degrees Celsius at 8000x the

force of gravity (g) for 20 minutes. The concentration of the precipitate, the RSV CA, will then be tested using the NanoDrop2000. This process will repeat until the desired concentration of 3mg/mL of RSV CA is reached. The RSV CA will be stored in a labeled micro-centrifuge tube.

Task 2: Track assembly of the RSV CA Via Turbidimetric Assay

The “Cell Cultures” program of the NanoDrop2000 spectrophotometer will be used to track the assembly of the RSV CA.

First, S75 buffer solution will be made according to Table 1.

Table 1: S75 buffer elements

10mM Tris-HCl pH 8.0
50mM NaCl
5mM 2-Mercaptoethanol (βME)

A 2μL drop of the S75 buffer will be pipetted onto the pedestal of the spectrophotometer and the spectrophotometer will be blanked. The pedestal will be wiped and cleaned with DI water.

Next, the RSV CA assembly will be initiated by combining equal volume of 1M sodium phosphate buffer at pH 8.0 using a ratio of 93.2 mL of 1M Na_2HPO_4 and 6.8 mL

of 1M NaH_2PO_4, to give a resulting protein solution of 500mM sodium phosphate buffer at pH 8.0 + 1.5 mg/mL RSV CA (~60 μM). Immediately upon assembly, the protein beginning to form into hexamers and pentamers, 2μL of the protein solution will be pipetted onto the NanoDrop2000 pedestal and the “Cell Cultures” program will be run. The optical density (OD) recordings will be taken starting at a wavelength of 250nm to 650nm at 50nm intervals. Results are recorded.

The “Cell Cultures” OD readings will be taken every 10 minutes in effort to monitor the assembly process. Once assembly begins to take place, new readings will be taken every 5 minutes until assembly ends. Readings will be taken every 10 minutes once assembly appears to have stopped until a total of 120 data points has been recorded. All collected data points will be graphed and analyzed using a data analysis software such as Excel.

Total time for the turbidimetric assay to complete is unknown, but expected to occur over a period of ~250 minutes with assembly occurring after a lag period of ~60 minutes and lasting ~200 minutes [6].

Task 3: Analyze the NMR spectra of the I190V mutation of RSV CA to determine the chemical shifts of the I190V mutant.

SsNMR spectra for the I190V mutation of RSV CA has been previously recorded by Dr. Xin Qiao. Using the software NMR Sparky, the chemical shifts for each of the 237 residues will be found and recorded. Once the chemical shifts have been found, the

program, TALOS-N, will be run to provide information and predictions on the secondary structure of the protein. This information will give us great insight into the structure of this mutated RSV CA. Depending on the chemical shifts recorded, we will be able to determine exactly what type of structure the RSV CA I190V mutant has.

Task 4: Analyze the torsion angles of the I190V mutant RSV CA and wild-type RSV CA to give insight into the different secondary structures that the I190V mutation brings.

Using the TALOS-N program, the chemical shifts of the I190V mutant RSV CA and wild-type RSV CA will be determined with given uncertainties. These torsion angles will then be plotted into Ramachandran plots to show the secondary structure of each residue. The differing torsion angles from the mutant and wild-type RSV CA will be compared to see how the I190V mutation affects the secondary structure of the protein.

RESULTS

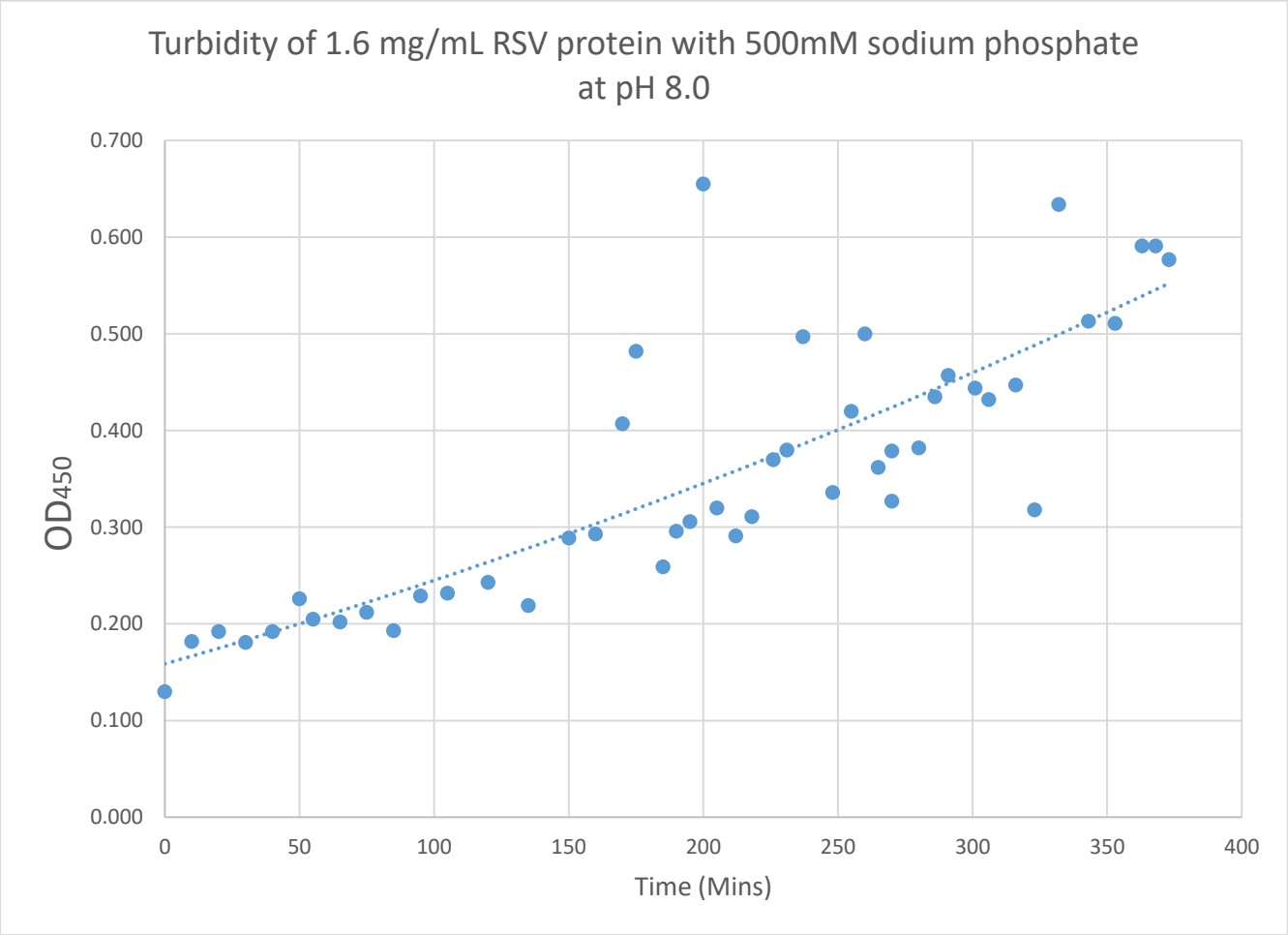

Figure 1: Turbidity assay of 1.6 mg/mL I190V RSV protein with 500mM $NaHOP_4$ salt at pH 8.0. The dotted line is a line of best fit.

Figure 1 shows the turbidity data for the I190V mutant RSV CA at 1.6mg/mL concentration in equal volume of 500mM sodium phosphate solution. The I190V mutated RSV CA behaves differently than the un-mutated, wild-type RSV CA. There was no notable lag period between addition of salt and assembly, as expected given the data collected from turbidity experiments on wild-type RSV CA [6].

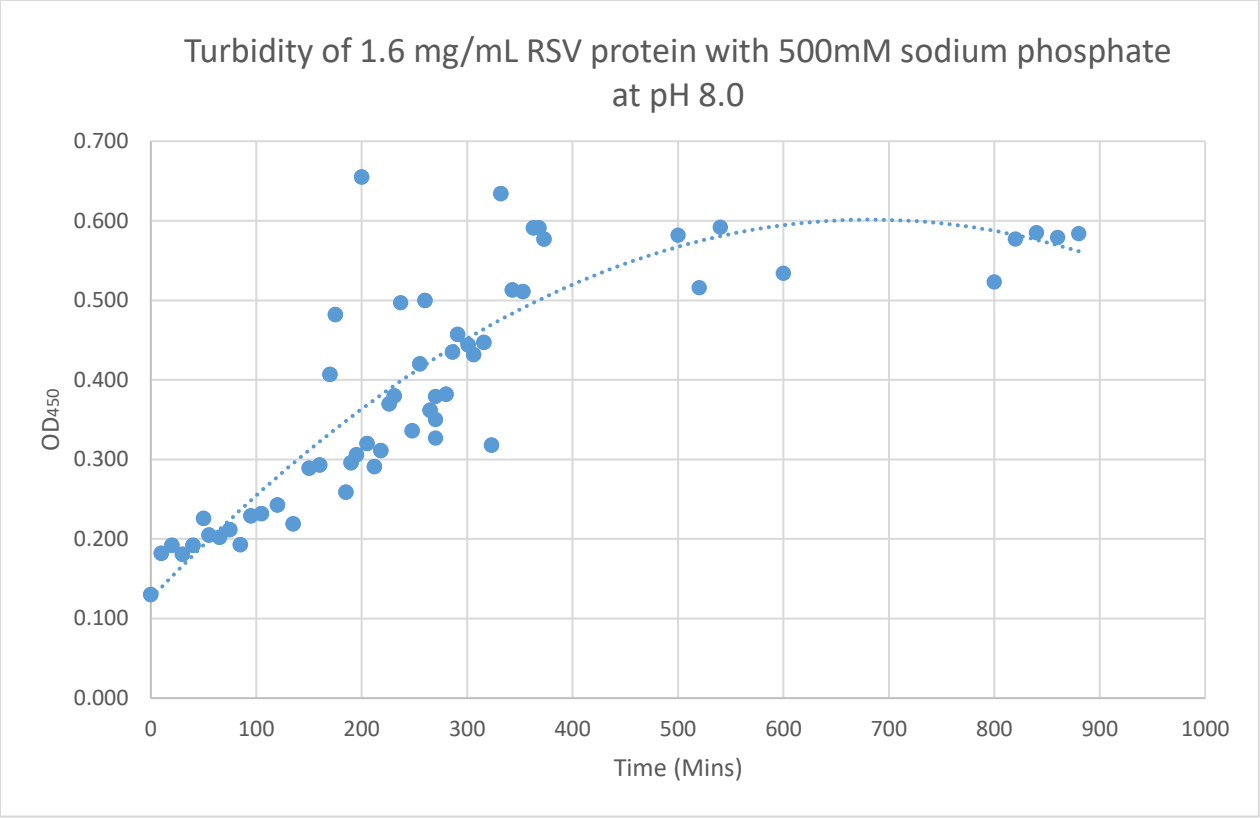

Figure 2: Turbidity assay of 1.6mg/mL I190v RSV CA with 500mM $NaHPO_4$ salt at pH 8.0 showing saturation. The dotted line is a line of best fit.

Figure 2 shows the same data as seen in Figure 1, however more data points are included. This shows us the time taken for the I190V mutated RSV CA to reach saturation. Saturation can be seen when the OD_{450} begins to level off, indicating there is no longer more proteins assembling together and changing the optical density.

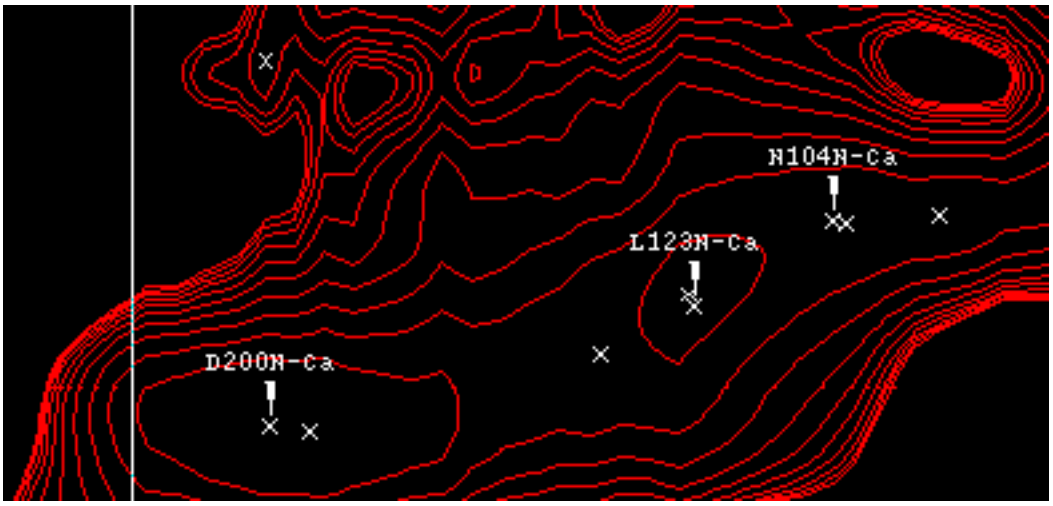

Image 3: Screenshot of the 2D NCaCx NMR spectra on the NMR Sparky software with some labeled peak assignments. NMR spectrum was acquired by previous student Xin Qiao.

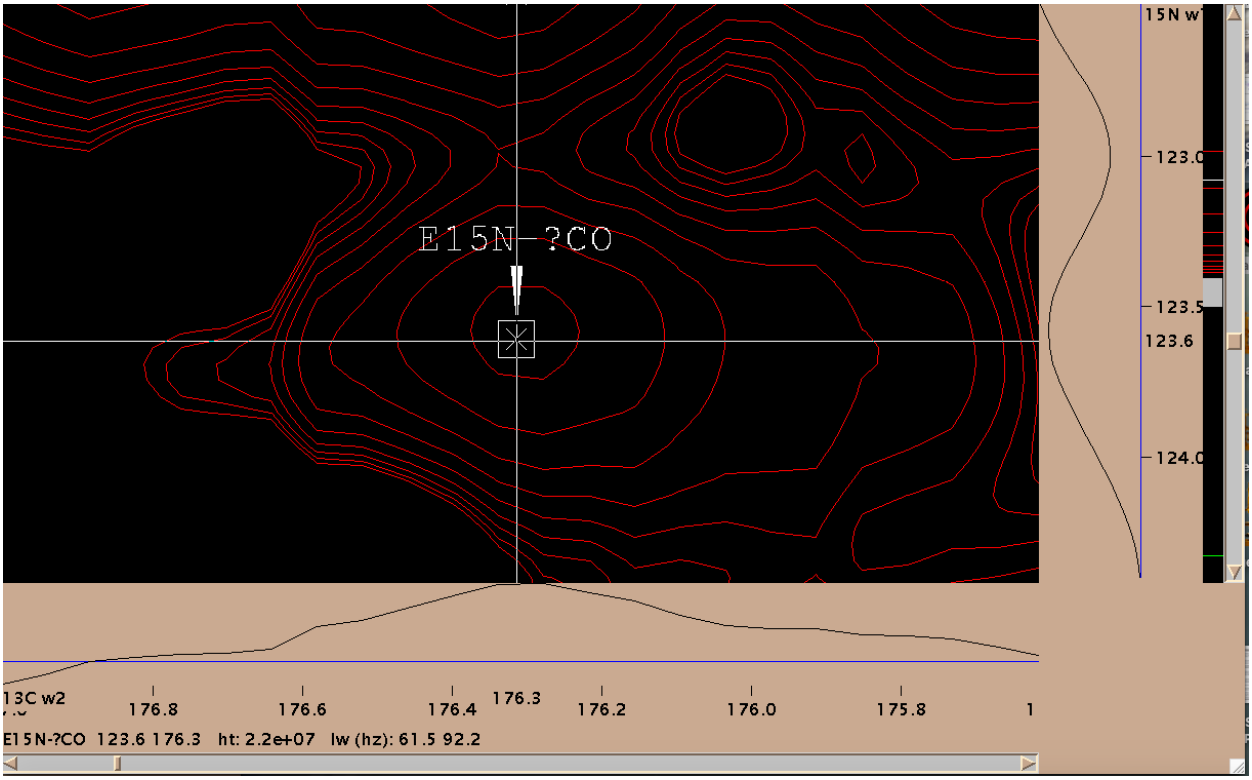

Image 4: A close up look at an individual peak of the 2DNCaCx NMR spectra on the NMR Sparky software. This peak corresponds to the carbonyl group of residue 15 of the 237 residue sequence of wild-type RSV CA. NMR spectrum was acquired by previous student Xin Qiao.

Tables 2 and 3

Tables 2 and 3 show the torsion angles, represented by the Phi and Psi angles, of the I190V mutated RSV CA (Table 2) and the wild type RSV CA (Table 3). Columns 4 and 8 represent the secondary structure shift of each residue. The residues with no filled information have not been found. Chemical shifts used to find torsion angles were found by previous student Xin Qiao.

Table 2

Residue	Phi Angle (°)	Psi Angle (°)	
1 P			
2 V			
3 V	-108 ± 7	128 ± 9	β
4 I	-90±7	124±9	
5 K	-103±11	131±13	β
6 T	-82±15	134±12	
7 E			
8 G			
9 P			
10 A			
11 W	-84±14	129±9	
12 T			
13 P			
14 L			
15 E			
16 P	-58±6	-32±5	α
17 K			
18 L	-67±7	-37±4	α
19 I	-68±4	-37±7	α
20 T	-65±4	-35±5	α
21 R	-65±4	-37±5	α
22 L	-69±5	-37±5	α
23 A	-67±7	-35±10	α
24 D	-65±4	-39±5	α
25 T	-65±4	-41±4	α
26 V	-64±4	-40±5	α
27 R	-64±3	-36±5	α
28 T	-75±11	-19±11	
29 K	-93±12	-2±13	
30 G	103±34	-4±31	
31 L	-73±12	-19±9	
32 R	-99±11	5±12	
33 S	-79±11	136±12	

Table 3

Residue	Phi Angle (°)	Psi Angle (°)	
1 P			
2 V	-110±9	132±7	β
3 V	-116±12	126±7	β
4 I	-90±8	120±12	
5 K	-95±12	-125±13	
6 T	-94±16	113±26	
7 E	-117±22	128±35	β
8 G	-154±45	178±14	β
9 P	-64±9	145±6	
10 A	-114±28	137±14	β
11 W	-82±16	129±9	
12 T	-124±13	132±17	β
13 P	-64±4	147±9	
14 L	-74±9	143±11	
15 E	-63±6	135±10	
16 P	-54±5	-35±5	α
17 K	-67±4	-37±5	α
18 L	-68±4	-40±4	α
19 I	-65±3	-41±5	α
20 T	-64±5	-41±5	α
21 R	-66±3	-40±4	α
22 L	-65±4	-43±4	α
23 A	-63±2	-40±4	α
24 D	-67±4	-37±4	α
25 T	-65±3	-42±3	α
26 V	-64±5	-42±5	α
27 R	-63±2	-36±4	α
28 T	-71±8	-18±9	
29 K	-92±14	-1±8	
30 G	98±8	4±7	
31 L	-71±2	-13±13	
32 R	-99±11	3±12	
33 S	-76±16	129±11	

34 P				34 P	-62±7	-27±9	α
35 I				35 I	-78±18	-18±27	
Table 2				Table 3			
36 T	-59±6	-36±8	α	36 T	-62±7	-40±7	α
37 M	-65±5	-37±5	α	37 M	-64±4	-40±6	α
38 A	-65±3	-40±3	α	38 A	-65±4	-39 ±4	α
39 E	-64±2	-42±4	α	39 E	-65±3	-40±5	α
40 V	-64±3	-41±2	α	40 V	-65±3	-41±3	α
41 E	-63±3	-41±4	α	41 E	-62±3	-41±5	α
42 A	-66±4	-39±5	α	42 A	-64±3	-41±4	α
43 L	-66±4	-33±5	α	43 L	-66±4	-33±6	α
44 M	-98±11	6±12		44 M	-90±8	-7±14	
45 S	-78±11	-19±12		45 S	-86±10	-15±8	
46 S	-65±8	-133±11		46 S	-71±10	136±11	
47 P				47 P	-64±7	137±10	
48 L				48 L	-127±26	143±14	β
49 L				49 L	-77±11	148±12	
50 P	-65±8	133±11		50 P	-53±3	-38±5	α
51 H	-58±5	-36±6	α	51 H	-66±4	-41±3	α
52 D	-64±4	-37±7	α	52 D	-67±4	-37±5	α
53 V	-67±5	-41±4	α	53 V	-65±2	-43±4	α
54 T	-63±2	-38±4	α	54 T	-63±4	-38±4	α
55 N	-65±3	-39±5	α	55 N	-66±3	-40±4	α
56 L	-66±4	-41±4	α	56 L	-65±3	-42±3	α
57 M	-66±4	-31±6	α	57 M	-67±4	-31±5	α
58 R	-63±6	-34±7	α	58 R	-67±4	-39±6	α
59 V	-68±7	-18±32		59 V	-68±6	-39±6	α
60 I				60 I	-77±8	-26±10	
61 L				61 L	-106±11	-14±11	
62 G				62 G	93±12	165±8	
63 P				63 P	-63±6	-34±7	α
64 A				64 A	-60±5	-49±4	α
65 P				65 P	-59±6	-37±5	α
66 Y	-80±17	36±62		66 Y	-65±5	-43±5	α
67 A	-59±5	-38±8	α	67 A	-66±2	-36±3	α
68 L	-64±5	-33±9	α	68 L	-66±5	-41±7	α
69 W	-73±11	-31±12	α	69 W	-65±5	-40±6	α
70 M	-69±11	-35±14	α	70 M	-66±3	-34±4	α
71 D	-58±26	-37±15	α	71 D	-67±4	-40±4	α
72 A	-62±5	-36±7	α	72 A	-67±4	-38±4	α
73 W	-67±8	-41±10	α	73 W	-66±4	-38±7	α
74 G	-60±5	-40±7	α	74 G	-63±3	-41±5	α

75 V	-66±3	-40±5	α	75 V	-64±2	-43±3	α
76 Q	-69±5	-38±6	α	76 Q	-64±4	-42±4	α
Table 2				Table 3			
77 L	-64±4	-39±5	α	77 L	-66±5	-40±4	α
78 Q	-65±2	-36±2	α	78 Q	-65±3	-37±4	α
79 T	-67±2	-39±3	α	79 T	-65±3	-40±4	α
80 V	-68±6	-37±8	α	80 V	-65±3	-43±4	α
81 I	-68±4	-32±5	α	81 I	-66±4	-36±4	α
82 A	-76±8	-21±9		82 A	-65±3	-39±5	α
83 A	-95±19	-6±21		83 A	-66±4	-36±5	α
84 A	-150±6	151±8	β	84 A	-66±4	-31±6	α
85 T	-108±13	130±8	β	85 T	-67±5	-30±7	α
86 R	-132±13	154±10	β	86 R	-83±9	-27±10	α
87 D	-102±37	126±28		87 D	-135±13	96±12	
88 P	-68±7	153±9		88 P	-64±7	-19±7	
89 R	-72±14	141±10		89 R	-90±11	-1±11	
90 H	-72±17	136±18		90 H	-68±10	130±8	
91 P	-65±8	144±23		91 P	-58±4	-30±8	α
92 A	-65±9	-24±10		92 A	-65±5	-26±6	
93 N	-105±6	9±9		93 N	-88±7	-11±11	
94 G	67±9	29±9		94 G	85±13	11±11	
95 Q	-95±19	-1±16		95 Q	-78±17	-17±14	
96 G	70±7	24±9		96 G	91±17	-1±15	
97 R	-90±16	-8±19		97 R	-65±7	138±10	
98 G	74±10	17±14		98 G	90±11	0±12	
99 E	-97±12	-14±11		99 E	-80±13	119±33	
100 R	-150±5	157±10	β	100 R	-73±14	142±14	
101 T	-96±21	167±12		101 T	-67±7	-22±7	
102 N	-64±7	-35±7	α	102 N	-104±7	13±10	
103 L	-79±16	-16±16		103 L	-57±5	-45±6	α
104 N	-66±7	-31±7	α	104 N	-64±4	-37±6	α
105 R	-101±17	-15±18		105 R	-64±5	-40±4	α
106 L	-73±16	-29±10		106 L	-69±6	-22±9	
107 K	-116±9	12±12		107 K	-101±10	-1±9	
108 G	78±16	17±15		108 G	67±5	28±7	
109 L	-90±13	59±41		109 L	-97±12	141±16	
110 A	-63±6	-36±7	α	110 A	-89±23	153±16	β
111 D	-63±6	-40±7	α	111 D	-58±3	131±5	
112 G	-65±5	-38±6	α	112 G	95±7	-10±11	
113 M	-63±6	-36±8	α	113 M	-80±14	137±13	
114 V	-80±14	-16±17		114 V	-66±9	124±8	

115 G	82±11	16±13		115	G	77±14	12±14	
116 N	-87±28	131±33		116	N	-130±16	83±14	
Table 2				Table 3				
117 P	-66±8	151±11		117	P	-61±4	-33±5	α
118 Q	-96±27	150±32	β	118	Q	-66±4	-41±4	α
119 G	-62±7	-35±7	α	119	G	-65±5	-40±5	α
120 Q	-69±10	-26±17		120	Q	-65±2	-40±2	α
121 A	-65±4	-29±10		121	A	-64±4	-37±5	α
122 A	-67±5	-30±11	α	122	A	-69±5	-27±7	
123 L	-74±8	-22±12		123	L	-82±13	-26±7	
124 L	-71±9	119±22		124	L	-71±14	143±12	
125 R	-99±32	135±25	β	125	R	-67±8	139±11	
126 P	-62±8	149±9		126	P	-53±3	-39±4	α
127 G	-59±5	-37±10	α	127	G	-63±5	-38±8	α
128 E	-65±10	-36±14	α	128	E	-69±4	-39±4	α
129 L	-65±7	-37±5	α	129	L	-56±3	-39±5	α
130 V	-65±4	-37±8	α	130	V	-64±3	-42±3	α
131 A	-65±6	-34±4	α	131	A	-65±3	-39±5	α
132 I	-66±5	-42±4	α	132	I	-65±4	-44±2	α
133 T	-66±3	-36±3	α	133	T	-63±2	-42±4	α
134 A	-66±3	-34±4	α	134	A	-64±3	-41±5	α
135 S	-67±5	-35±3	α	135	S	-64±2	-40±3	α
136 A	-68±4	-37±5	α	136	A	-65±2	-40±3	α
137 L	-66±3	-35±3	α	137	L	-65±3	-41±4	α
138 Q	-66±3	-37±3	α	138	Q	-67±3	-36±4	α
139 A	-66±3	-38±4	α	139	A	-66±3	-40±4	α
140 F	-67±3	-35±3	α	140	F	-64±3	-43±3	α
141 R	-66±3	-38±4	α	141	R	-64±3	-38±5	α
142 E	-67±3	-35±5	α	142	E	-65±2	-39±5	α
143 V	-72±9	-27±7		143	V	-66±3	-41±4	α
144 A	-84±10	-20±16		144	A	-64±3	-38±5	α
145 R	-122±19	145±14	β	145	R	-68±4	-34±5	α
146 L	-79±13	126±16		146	L	-82±7	-21±10	
147 A				147	A	-74±9	131±11	
148 E				148	E	-68±5	139±11	
149 P				149	P	-66±7	150±12	
150 A				150	A	-75±19	153±21	
151 G	84±15	-169±17		151	G	-55±12	-55±7	α
152 P	-69±10	154±17		152	P	-59±8	-35±7	α
153 W	-91±17	39±53		153	W	-62±5	-45±4	α
154 A	-128±28	158±15	β	154	A	-64±3	-37±4	α
155 D	-98±23	125±24	β	155	D	-67±4	-37±6	α

156 I				156	I	-65±4	-43±4	α
157 M	-103±26	133±14		157	M	-64±5	-38±9	α
Table 2				Table 3				
158 Q				158	Q	-77±13	-15±19	
159 G	120±35	-176±12		159	G	88±20	176±28	
160 P	-64±10	151±11		160	P	-65±7	-25±8	
161 S	-78±13	120±35		161	S	-96±15	9±17	
162 E	-94±34	128±9	β	162	E	-103±22	133±10	β
163 S	56±9	39±13		163	S	-67±7	146±12	
164 F	-76±11	-28±12		164	F	-56±5	-42±5	α
165 V	-125±16	154±12	β	165	V	-63±3	-41±5	α
166 D	-71±12	126±15	β	166	D	-67±4	-38±4	α
167 F	-75±19	-20±20		167	F	-65±3	-42±4	α
168 A	-59±6	-42±7	α	168	A	-64±1	-39±3	α
169 N	-60±4	-33±6	α	169	N	-64±3	-41±4	α
170 R	-63±4	-38±5	α	170	R	-64±4	-43±4	α
171 L	-66±4	-38±6	α	171	L	-64±3	-42±3	α
172 I	-65±5	-35±4	α	172	I	-62±2	-43±3	α
173 K	-67±5	-34±7	α	173	K	-63±4	-40±5	α
174 A	-74±17	-32±14	α	174	A	-64±3	-41±4	α
175 V	-92±25	-10±28		175	V	-65±5	-40±6	α
176 E	-154±17	159±19	β	176	E	-68±7	-30±8	α
177 G	77±17	-137±17		177	G	-81±9	-11±19	
178 S	-58±94	73±78		178	S	-89±26	152±16	
179 D	-92±15	-5±21		179	D	-86±9	-6±12	
180 L				180	L	-68±7	136±9	
181 P				181	P	-60±6	141±12	
182 P	-61±6	145±8		182	P	-53±4	-37±5	α
183 S	64±4	24±10		183	S	-69±4	-18±9	
184 A	-89±34	139±19		184	A	-106±11	0±11	
185 R	-81±25	-22±26		185	R	-62±6	-44±7	α
186 A	-84±29	145±16		186	A	-63±3	-48±4	α
187 P				187	P	-61±3	-36±5	α
188 V				188	V	-63±3	-42±3	α
189 I				189	I	-63±2	-44±3	α
190 V	-122±9	157±14	β	190	I	-63±3	-37±6	α
191 D	-156±89	118±28	β	191	D	-66±3	-36±4	α
192 C	-62±8	-29±8	α	192	C	-68±6	-34±9	α
193 F	-71±10	-28±15		193	F	-67±5	-41±4	α
194 R	-74±11	-19±11		194	R	-66±4	-35±7	α
195 Q	-99±14	-3±17		195	Q	-78±12	-19±12	
196 K	-70±10	142±12		196	K	-77±13	139±28	

197 S				197	S	-76±8	162±11	
198 Q	-73±14	141±13		198	Q	-66±5	144±11	
Table 2				Table 3				
199 P				199	P	-54±4	-41±4	α
200 D	-79±13	101±17		200	D	-69±4	-35±5	α
201 I	-69±12	-24±15		201	I	-67±3	-39±5	α
202 Q	-61±5	-38±7	α	202	Q	-62±2	-41±4	α
203 Q	-74±12	-21±13		203	Q	-64±4	-40±4	α
204 L	-83±17	-18±21		204	L	-65±3	-42±4	α
205 I				205	I	-63±3	-40±5	α
206 R	-96±16	125±10	β	206	R	-68±5	-36±8	α
207 T				207	T	-71±5	-31±8	α
208 A	-73±10	151±15		208	A	-89±34	127±26	
209 P	-67±9	152±10		209	P	-63±4	145±6	
210 S	-75±18	132±14		210	S	-92±38	152±19	
211 T	-129±9	152±11	β	211	T	-68±6	-33±7	α
212 L	-134±10	149±10	β	212	L	-130±14	144±11	β
213 T				213	T	-112±25	-5±23	
214 T				214	T	-136±25	161±6	β
215 P				215	P	-58±4	-37±5	α
216 G				216	G	-63±5	-40±5	α
217 E	-61±5	-35±5	α	217	E	-66±3	-38±5	α
218 I	-69±6	-38±7	α	218	I	-67±3	-37±5	α
219 I	-71±10	-21±15		219	I	-63±4	-43±4	α
220 K				220	K	-63±2	-38±4	α
221 Y				221	Y	-64±6	-44±2	α
222 V	-114±16	156±10	β	222	V	-63±3	-42±3	α
223 L	-59±6	-35±4	α	223	L	-65±3	-40±4	α
224 D	-65±6	-33±9	α	224	D	-66±3	-40±5	α
225 R	-74±9	-26±11		225	R	-67±5	-35±6	α
226 Q	-80±15	-27±17		226	Q	-67±4	-33±4	α
227 K	-146±9	159±9	β	227	K	-70±8	-26±9	
228 T				228	T	-96±14	44±57	
229 A				229	A	-70±8	137±12	
230 P				230	P			
231 L				231	L			
232 T				232	T			
233 D				233	D			
234 Q				234	Q			
235 G				235	G	-66±8	-28±10	α
236 I				236	I	-91±17	137±13	
237 A				237	A	238		

Each residue has been labeled as α-helix (α) or β-sheet (β) in the fourth column of Table 3 and Table 4. The average values for α-helices are clustered around ϕ=-57° and ψ=-47°, while the average values for β-sheets are clustered around ϕ=-130° and ψ=140°. Some of the residues secondary structure cannot be reasonably determined as α-helix or β-sheet. For example, the 93rd residue, Asparagine, has ϕ angle value of -105±6 and ψ angle value of 9±9, which do not fall into the accepted range for α-helix or β-sheet. When comparing the secondary structure of the residues in the spherically assembled RSV CA (column 4) to the secondary structure of the tubular RSV CA (column 8) some discrepancies can be seen. This indicates that when the RSV CA assembles into spheres versus tubes there is in fact notable secondary shifts in structure from α-helix to β-sheet and vice versa in some residues.

These secondary structure shifts can also be seen when the ϕ angles are plotted against the ψ angles in Ramachandran plots. The α-helix residues will be clustered together around the average α-helix ϕ and ψ values of -57° and -47° respectively, while the β-sheet residues will be clustered around the average ϕ and ψ values for β-sheet of -130° and 140° respectively. The Ramachandran plots can be seen below in Figure 3 and 4.

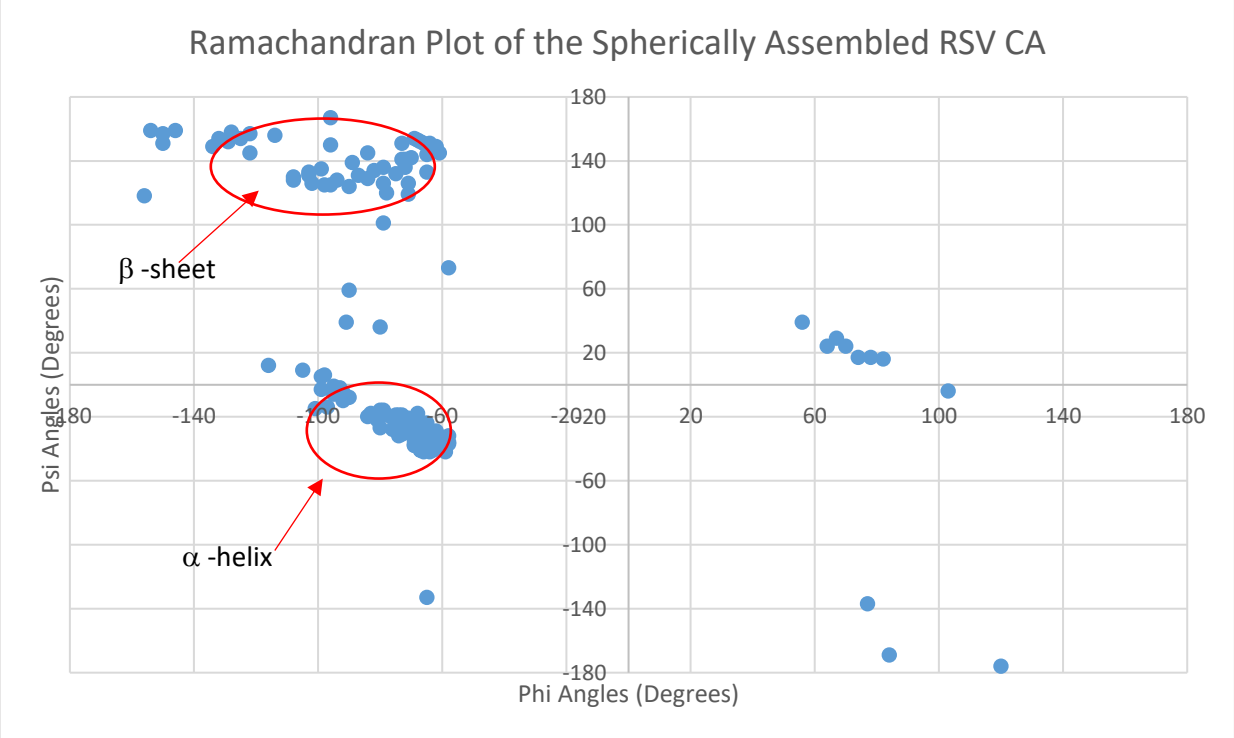

Figure 3: Figure 3 shows a Ramachandran plot of the Spherically Assembled mutant RSV CA. The Ramachandran plot graphs the torsion angles of each residue given their respective chemical shifts.

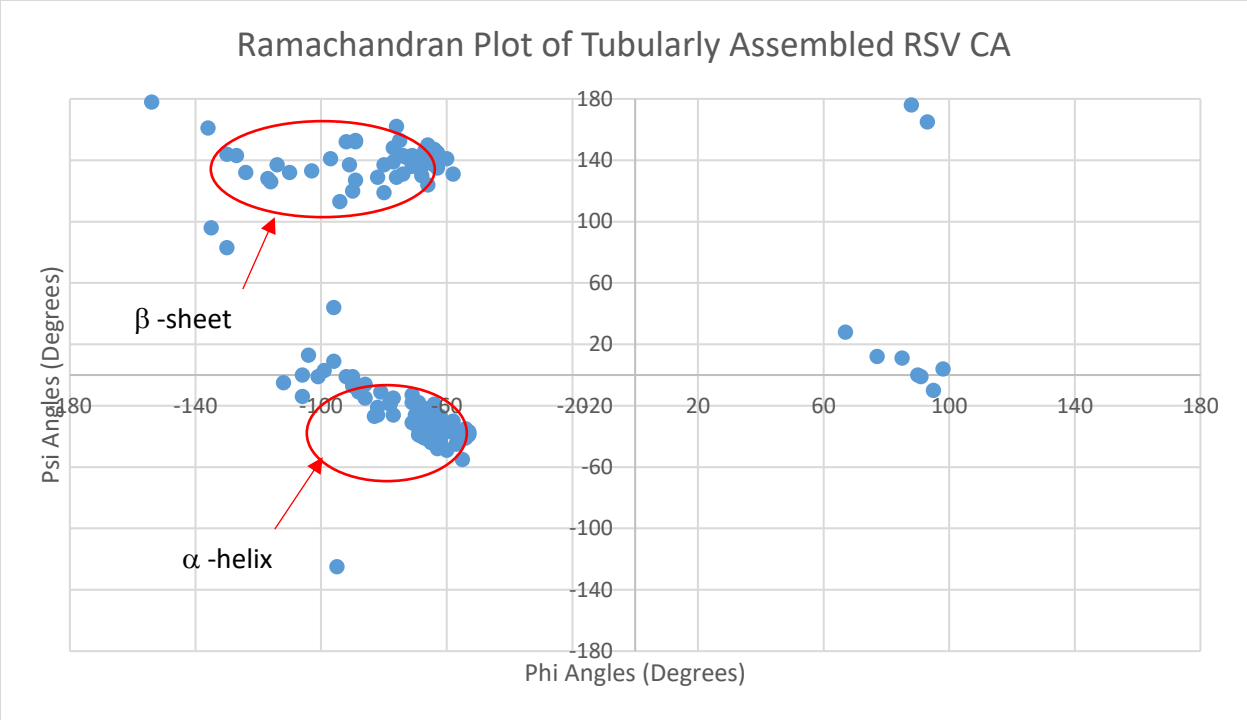

Figure4: Figure 4 shows a Ramachandran plot of the Tubular wild-type RSV CA. The Ramachandran plot graphs the torsion angles of each residue given their respective chemical shifts.

To see where in the residue sequence the secondary structures differ between the spherical and tubular RSV CA, the differences between the ϕ angles ($\Delta\phi$) and ψ angles ($\Delta\psi$) of the spherical and tubular RSV CAs were plotted in Figure 5 and Figure 6. Where there is no difference, and hence no change in torsion angle resulting in no change of secondary structure, the data points will lie on or around the x-axis. Where the torsion angles between the spherical and tubular RSV CAs differ greatly, and hence indicate a change in secondary structure are seen in the data points that fall a great distance from the x-axis.

Further, on both Figure 5 and Figure 6, the range of residues that fall within the eleven helices and one 3_{10} helix that form the structure of the RSV CA can be seen by red transparent rectangles. The first rectangle representing the first helix (H1) and the last representing H11.

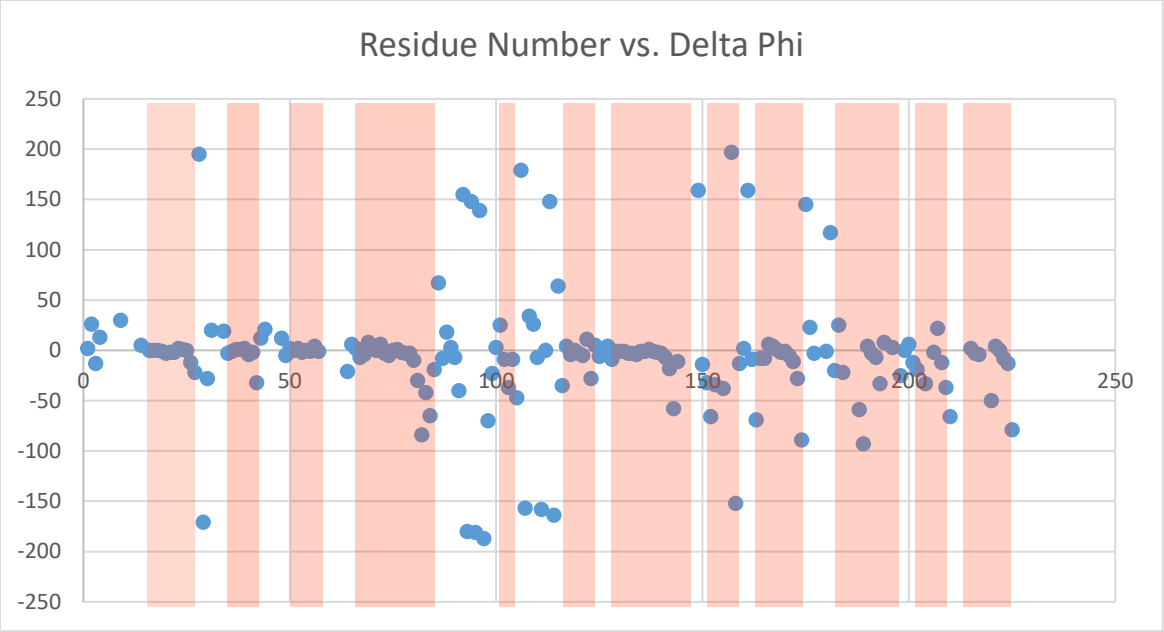

Figure 5: Figure 5 compares the phi angles of the spherical mutant RSV CA and the tubular wild-type RSV CA by plotting the difference between each mutated RSV CA residue's phi angles compared to the corresponding residue's phi angles in the wild-type RSV CA. The red transparent rectangles represent the residues that fall in the range of each of the eleven helices and short 3_{10} helix (residues 152 – 158).

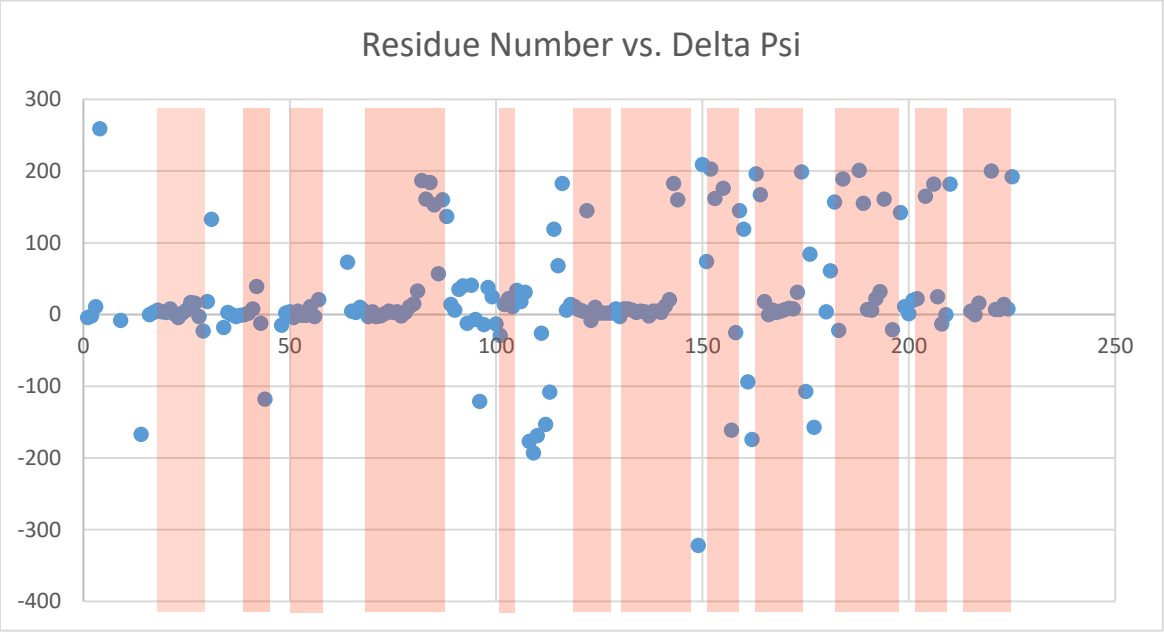

Figure 6: Figure 6 compares the psi angles of the spherical mutant RSV CA and the tubular wild-type RSV CA by plotting the difference between each mutated RSV CA residue's psi angles compared to the corresponding residue's psi angles in the wild-type RSV CA. The red transparent rectangles represent the residues that fall in the range of each of the eleven helices and short 3_{10} helix (residues 152 – 158).

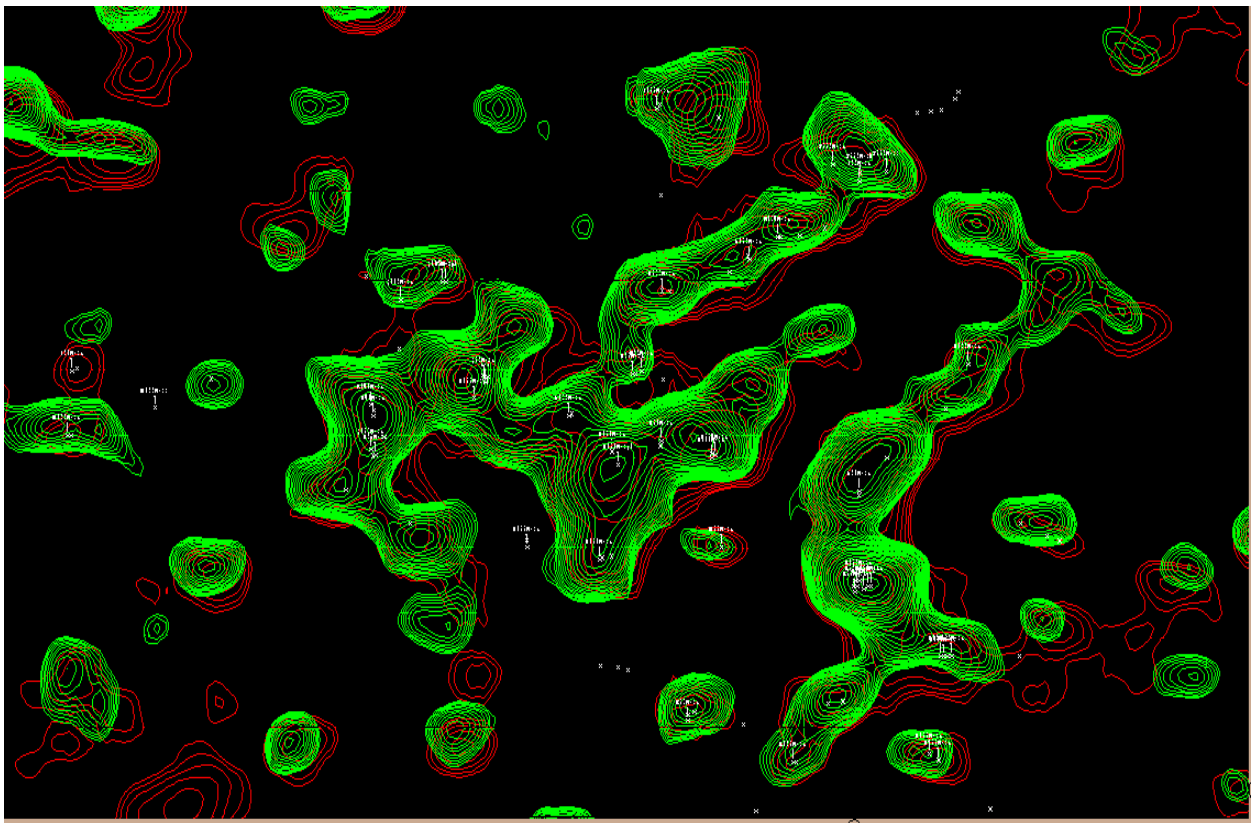

Image 5: Screenshot of the tubular wild-type RSV CA (green) overlaid on to the mutant RSV CA (red) showing relative but not perfect alignment on a broad scale. NMR spectra were acquired by previous student Xin Qiao.

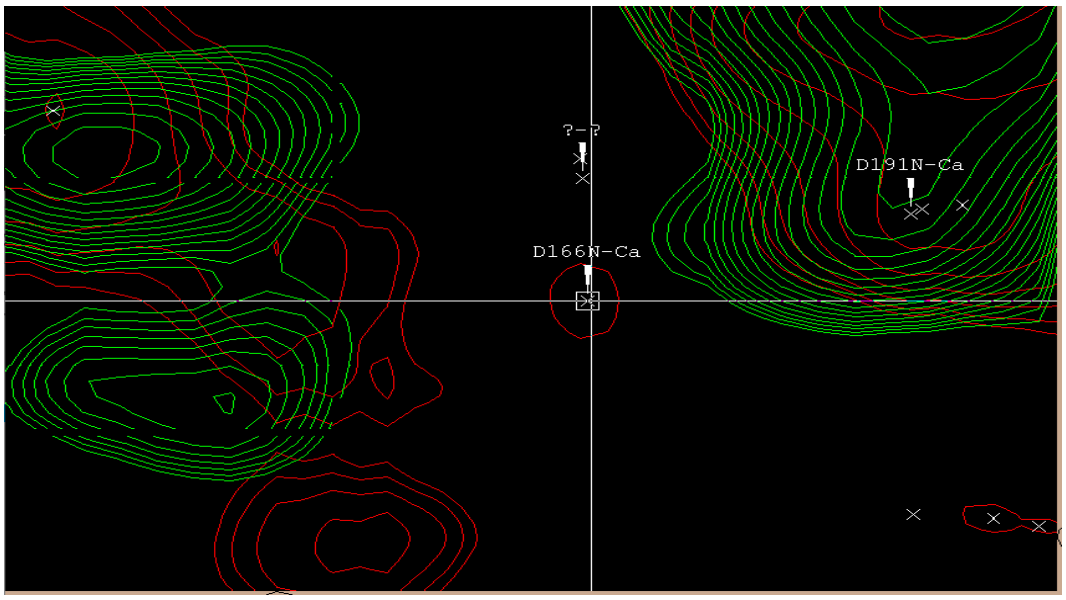

Image 6: The peak of residue 166 in the mutant RSV CA does not align with any wild-type RSV CA residue. NMR spectra were acquired by previous student Xin Qiao.

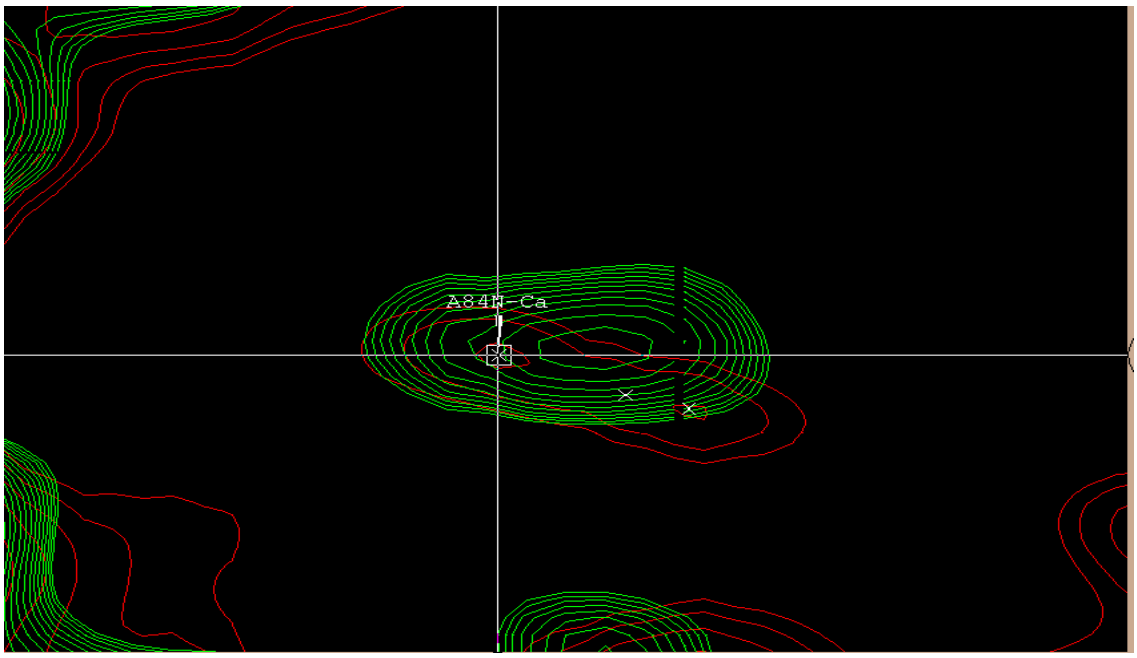

Image 7: The C^{α} peak of residue 84 of the mutant RSV CA (red) overlaid by the tubular wild-type RSV CA (green). NMR spectra were acquired by previous student Xin Qiao.

To further show the discrepancies in the NMR spectra of the spherically assembled mutant RSV CA and the tubular wild-type, the 2DNCaCx NMR spectra were overlaid and can be seen above. The red contour lines represent the spherical RSV CA while the green contour lines represent the tubular RSV CA.

DISCUSSION

Figure 1 shows the turbidity data for the I190V mutant RSV CA at 1.6mg/mL concentration in equal volume of 500mM sodium phosphate solution. The I190V mutated RSV CA behaves differently than the un-mutated, wild-type RSV CA. There was no notable lag period between addition of salt and assembly, as expected given the data collected from turbidity experiments on wild-type RSV CA [6]. The lack of a noticeable lag period is due to a number of factors. One factor is that the RSV CA used in the Purdy paper was the wild-type RSV CA. In other words, Purdy's study was on the un-mutated strain of RSV CA. The I190V mutation is an amino acid replacement mutation, replacing the 190th residue of Isoleucine with Valine. This mutation in the RSV CA residue sequence can affect how the protein behaves. The full structure of the I190V mutated RSV CA is investigated later on in this thesis. Another factor that could lead to the turbidity assay of the I190V mutated RSV CA are the assembly variables used. This includes concentration of protein before assembly is induced, as well as the concentration of salt solution used to induce assembly. In this thesis, the I190V mutated RSV CA was brought to a concentration of 3.2 mg/mL via centrifugation. After being mixed with equal volume of salt solution to induce assembly, the final protein concentration was 1.6 mg/mL. In other literature, such as the Purdy paper[6], varying concentrations of protein were used in turbidity assays. The closest concentration to the concentration used in this thesis was 120 μM, roughly equivalent to 3.06 mg/mL, before addition of equal volume of buffer. The concentration used in this thesis is slightly higher than the 120μM used in the Purdy paper, which showed vary little lag time before assembly began. [6] However, 120μM of wild-type RSV CA began to level off, or

reached saturation, at the ~120 minute mark. The I190V mutated RSV CA did not show any sign of saturation until around the 600-minute mark, as seen in Figure 2. The concentration of salt, as well as type of salt used to induce assembly, sodium phosphate buffer at pH 8.0, were the same as literature [6]. This tells us the differing assembly behavior of the I190V as shown through turbidity assay is due to the mutation of the 190th residue.

The goal of the turbidity experiments to observe the assembly of the I190V mutated RSV CA into spheres, versus the tubular structure that RSV CA can also assemble into under different parameters. NMR spectra of spherically assembled wild-type RSV CA was obtained and analyzed using the NMR Sparky software to understand the structurally differences of RSV CA between tubular and spherical assembly. Table 2 contains all 237 residues of the wild-type RSV CA, with the last 10 residues being unassigned. The structure of this spherically assembled RSV CA is analyzed by recording the C^{α}, CO, C^{β}, C^{γ}, C^{δ}, C^{ε}, and aromatic chemical shifts. The values for the corresponding chemical shifts of the 237 residues were found using NMR Sparky. The NMR spectra of the wild-type RSV CA are seen in Images 3 and 4. Image 3 is a close up of one particular CO peak of the 15th residue in the wild-type RSV CA sequence, glutamic.

The chemical shift data was then analyzed further using the TALOS-N software. What this software does is use secondary chemical shift and sequence information of a protein to make quantitative predictions for the protein back bone angles ϕ/ψ, and then provide a measure of the uncertainties in these predictions.

These ϕ and ψ angles were plotted into Ramachandran plots where clustering of certain angles tell us about the secondary structure of the protein, and whether or not each residue is alpha-helix or beta-sheet. The average values for α-helices are clustered around ϕ=-57° and ψ=-47°, while the average values for β-sheets are clustered around ϕ=-130° and ψ=140°. [14] Each residue has been labeled as α-helix (α) or β-sheet (β) in the fourth column of Table 3 and Table 4. Some of the residues secondary structure cannot be reasonably determined as α-helix or β-sheet. For example, the 93rd residue, Asparagine, has ϕ angle value of -105±6 and ψ angle value of 9±9, which do not fall into the accepted range for α-helix or β-sheet. Reasons as to why some residues cannot be labeled as α-helix or β-sheet occur when the residues are in the loop or random coil region in between segments of α-helix and β-sheet.

When comparing the torsion angles of the mutated, spherically assembled RSV CA to the wild-type, tubular assembled RSV CA, there are some notable differences. Most of the residues have the same secondary structure, that is there ϕ and ψ angles are the same. For example, the 25th residue, threonine, in the mutated RSV CA has ϕ angle of -65±5 and ψ angle of -41±4. This same, 25th residue, in the wild type RSV CA has a ϕ angle of -65±3 and ψ angle of -42±3. These are virtually the exact same torsion angles given their minor uncertainties. However, if you look at the 84th residue, Alanine, in the mutated RSV CA, a ϕ angle of -150±6 and ψ angle of +151±8 is found. Comparing these angles to the ϕ angle of -66±4 and ψ angle of -31±6 in the wild-type RSV CA, a drastic difference can be seen. The 84th residue of the mutated RSV CA is β-sheet shifted, while the 84th residue in the wild-type RSV CA is α-helix shifted. A

mutation of a residue over a 100 residues away in the sequence of RSV CA can drastically affect the secondary structure of residues throughout the protein. Similar discrepancies can be found throughout the residue sequences of the I190V mutated RSV CA and the wild-type RSV CA. Thus, a single mutation in the residue sequence of a protein can drastically affect how the protein assembles.

Many of these discrepancies between torsion angles of the mutated RSV CA and the wild-type RSV CA occur at helices that help make up the structure of RSV CA. For example, along the boundary of helix 9 and 10, the 191st residue, Aspartate, is β-sheet in the mutated RSV CA but α-helix in the wild-type RSV CA. Similarly, the 206th residue, Arginine, and the 211th residue, Threonine, are both β-sheet in the mutated RSV CA along helix 11, but are α-helix in the wild-type RSV CA. The string of residues 84, 85, and 86 in the mutated RSV CA are β-sheet while α-helix in the wild-type RSV CA. These three residues lie along helix 5. Similar changes in secondary structure of the mutant RSV CA occur throughout the residue sequence at these helices. At the interface of helices 4, 8, and 11 are in close contact in the structure of the tubular RSV CA. Helix 4 consists of residues 64-86, Helix 8 consists of residues 163-177, and Helix 11 consists of residues 214-226. As seen in Table 2, there are changes in secondary structure in the mutant RSV CA at the boundaries of these residue ranges. This means that this NTD-CTD interface exhibits changes to reform the hexamer or pentamer combination. It is safe to say many of the changes in the secondary structure of the mutant RSV CA are localized in the loops between helices.

The 2DNCaCx NMR spectra of the wild-type RSV CA was overlaid on to the 2DNCaCx NMR spectra of the mutated RSV CA. As seen in Image 5, the spectra align

reasonably well, however, they do not align perfectly. There are many peaks of the mutant RSV CA that are shifted along the 13C or 15N axes when compared to their corresponding residue peaks of the wild-type RSV CA. In Image 7, a misalignment of the 84th residue, Alanine is shown. This misalignment of peaks between the two NMR spectra also correspond to a difference in secondary structure. In the mutated RSV CA, the 84th residue is β-sheet, however, it is α-helix in the wild-type RSV CA. Image _ shows the misalignment of the 165th residue, Valine, that also corresponds to a different secondary structure where this residue is β-sheet in the mutated RSV CA, but α-helix in the wild-type. Image 6, shows residue 166, Aspartic Acid, corresponds to a peak that is separate from any tubular peak. This would occur due a shift in secondary structure of the 166th residue in the mutated RSV CA. This is further evidence that the mutation of the 190th residue from Isoleucine to Valine has altered the structure of the CA.

The spherically assembled I190V mutated RSV CA has a lack of a noticeable lag period before the initiation of the assembly process following the introduction of sodium phosphate solution, as well as, takes ~400 minutes longer to reach saturation. The spherically assembled mutated RSV CA displays secondary structure shifts from α-helix to β-sheet and vice versa when compared to the tubular wild-type RSV CA. These secondary structure shifts are concentrated at key helix interfaces, such as the interface of helix 4, 8, and 11. A noticeable difference in assembly process and in the structure of spherically assembled RSV CA when compared to the tubular assembled RSV CA has been found. Previous attempts to distinguish differences like these between capsid proteins of similar molecular structure, such as the HIV capsid protein, has not been found.

LIST OF REFERENCES

[1] Withers, Johanna B. and Beemon, Karen L. “The structure and function of the rous sarcoma virus RNA stability element.” Journal of Cellular Biochemistry, Issue 11, Volume 112, 2011.

[2] Bailey, Graham D., Hyun, Jae K., Mitra, Alok K., Kingston, Richard L. “Proton-Linked Dimerization of a Retroviral Capsid Protein Initiates Capsid Assembly.” Structure, Issue 17, 2009, pp. 737-748.

[3] Tsiang, Manuel, Niedziela-Majka, Anita, Hung, Magdeleine, Jin, Debi, Hu, Eric, Yant, Stephen, Samuel, Dharmaraj, Liu, Xiaohong, Sakowicz, Roman. “A Trimer of Dimers is the Basic Building Block for Human Immunodeficiency Virus-1 Capsid Assembly.” Biochemistry, 2012, pp. 4416-4428.

[4] Fan,Hung. “Retroviruses.” Encyclopedia of Microbiology, Third Edition, 2009, pp. 519-534.

[5] Darlix, Jean-Luc, Lapadat-Tapolsky, Mary, de Rocquigny, Hugues, Roques, Bernard P. “First Glimpses at Structure-function Relationships of the Nucleocapsid Protein of Retroviruses.” Journal of Molecular Biology, Volume 254, Issue 4, 1995, pp. 523-537.

[6] Purdy, John G., Flanagan, John M., Ropson, Ira J., Craven, Rebecca C. “Retroviral Capsid Assembly: A Role for the CA Dimer in Initiation.” Journal of Molecular Biology, Volume 389, 2009, pp. 438-451.

[7] Maclachlan, N. J., Dubovi, Edward J., Barthold, Stephen W., Winton, Swayne and James R. “Retroviridae” Fenner’s Veterinary Virology, Fifth Edition, Chapter 15, 2016, pp.299-317.

[8] Crick, F. H. C. “On Protein Synthesis.” Symposia of the Society for Experimental Biology, 1958, pp. 138-161.

[9] Bischoff, Rainer, Schulter, Hartmut. “Amino acids: Chemistry, functionality and selected non-enzymatic post-translational modifications.” Journal of Proteomics, Volume 75, Issue 8, 2012, pp.2275-2296.

[10] Liu, Jingxian, Song, Jingxing. “Insights into Protein Aggregation by NMR Characterization of Insoluble SH3 Mutants Solubilized in Salt-Free Water.” PLoS One, 2009, Volume 4, Issue 11.

[11] Edwards, John C. “Principles of NMR.” Process NMR Associates LLC, 2009, pp. 1-51.

[12] Opella, S. J., Nevzorov, A., Mesleh, M.F., Marassi, F.M. “Structure determination of membrane proteins by NMR spectroscopy” NIH Public Access, 2002

[13] Hore, P. J. “Nuclear Magnetic Resonance” Oxford University Press, 2015.

[14] Hollingsworth, S. A., Karplus, P. A. “A fresh look at the Ramachandran plot and the occurrence of standard structures in proteins” HHS Public Access, Biomol Concepts, 2010, pp. 271-283.

[15] Polenova, T., Gupta, R., Goldbourt, A. “Magic Angle Spinning NMR Spectroscopy: A Versatile Technique for Structural and Dynamic Analysis of Solid-Phase Systems.” HHS Public Access, Anal Chem, 2015, pp. 5458-5469.